ACOUSTIC INVERSION BY A RMS BORN APPROXIMATION SPACE - TIME DOMAIN

JACOB TJEERD FOKKEMA

Programa de Pesquisa e Pós-Graduação em Geofísica
da Universidade Federal da Bahia
Campus Universitário da Federação
CEP. 40.210 - SALVADOR - BAHIA

and

PETER M. VAN DEN BERG

Laboratory of Eletromagnetic Research
Department of Eletrical Engineering
Delft University of Technology
P.O. Box 5031, 2.600 GA Delft
The Metherlands

ABSTRACT

A new approximate method to calculate the space-time acoustic wave motion generated by an impulsive point source in a horizontally layered configuration is presented. The configuration consists of a stack of fluid layers between two acoustic half-spaces where the source and the receiver are located in the upper half-space. A distorted-wave Born approximation is introduced; the important feature of the present method is the assumption of the presence of a background medium with vertical varying root-mean-square acoustic wave speed. A closed-form expression for the scattered field in space and time as a function of the contrast parameters is arrived at. The result is in close agreement with synthetic seismograms calculated in a rigorous way. In the inverse scheme the wave speed and mass density can be reconstructed within a single trace. Results of the inversion scheme applied to synthetic data have been shown.

1. INTRODUCTION

The ordinary Born approximation is widely used to simplify both forward and inverse problems of wave propagation models for seismic exploration (Cohen and Bleistein 1977,1979; Phinney and Frazer 1978; Raz 1981a,b). Within this Born approximation, the solution of the acoustic wave equation is expressed as a perturbation about a known solution to the simple equations of a homogeneous background medium. The Born approximation is a low-contrast approximation in the integral equation governing the total scattering mechanism of the acoustic waves in the configuration. In this paper, we derive a closed-form expression in the space-time domain. However, the inherent use of a constant background medium leads to incorrect arrival times.

In the distorted-wave approximation (Beylkin and Oristaglio 1985) we assume a more realistic inhomogeneous background medium. In most cases, the field solution of a point source is then difficult to obtain and complicated inversion schemes are the results of it (Clayton and Stolt 1981, Foster and Carrion 1984, Bleistein and Gray 1985, Weglein, Violette and Keho 1986).

In the present paper where we deal with a horizontally layered configuration, we take an inhomogeneous background medium in such a way that a very simple approximate solution to the problem of a point-source in this background medium is arrived at. The precise assumption of the structure of the background medium is circumvented by deriving a closed-form low-contrast approximation of the analytical expression in the Laplace-Fourier transform domain of the Cagniard-De Hoop technique (De Hoop 1960, Aki and Richards 1980) with primaries only (Drijkoningen and Fokkema 1987). It appears that we have arrived at a distorted-wave Born approximation with some vertical varying root-mean-square acoustic wave speed. Some numerical results of the

present forward problem are presented and compared with the results of the exact Cagniard-De Hoop technique.

Further, we show that our RMS Born approximation leads to a very simple inversion scheme, where the two constitutive parameters, the mass density and the wave speed, of the fluid layers can simultaneously be reconstructed within a single trace. We finally present some results of the inversion scheme applied to synthetic data of the Cagniard-De Hoop technique.

2. DESCRIPTION OF CONFIGURATION

The Cartesian coordinates $\{x_1,x_2,x_3\}$ with respect to the right-handed orthogonal Cartesian reference frame $\{\underset{\sim}{i}_1,\underset{\sim}{i}_2,\underset{\sim}{i}_3\}$ locate a point in space, while t represents the time of observation. The vectors and tensors which occur are given in subscript representation. Lower-case Latin subscripts are used for this purpose; they are assigned the values 1, 2 and 3. The summation convention applies to repeated subscripts. Partial differentation with respect to x_k is denoted by ∂_k; the symbol ∂_t denotes the partial derivative with respect to time. SI units are used throughout.

We consider a horizontally stratified linear acoustic medium in the vertical x_3-direction. The acoustic properties of the configuration are characterized by its volume density of mass ρ and its compressibility κ. Both ρ and κ are functions of x_3. They are independent of the horizontal coordinates x_1, x_2, and the time coordinate t. The functions $\rho = \rho(x_3)$ and $\kappa = \kappa(x_3)$ are taken piecewise constant (Fig.1). The related acoustic wave speed is given by

$$c = (\rho\kappa)^{-1/2} > 0. \tag{2.1}$$

An impulsive point source at $\{0,0,x_3^{(S)}\}$ generates the acoustic waves. This source starts to act at $t = 0$. A receiver is located at $\{x_1^{(R)},x_2^{(R)},x_3^{(R)}\}$. We consider the case that both source and receiver are located in the upper homogeneous half-space with $\rho = \rho_0$, $\kappa = \kappa_0$ and $c = c_0$ (Fig.1). The latter model is of extreme importance in land and marine seismics.

3. BASIC ACOUSTIC WAVE EQUATIONS

The equations that govern the linearized acoustic wave motion in a fluid are the equation of motion

$$\partial_k p + \rho\, \partial_t v_k = f_k^i, \tag{3.1}$$

and the deformation equation

$$\partial_k v_k + \kappa\, \partial_t p = q^i. \tag{3.2}$$

In these equations p is the acoustic pressure, v_k is the particle velocity, f_k^i is the volume source density of force, and q^i is the injection rate. We consider a point source located at $\{0,0,x_3^{(S)}\}$ with vertical force strength F(t) and injection rate strength Q(t). Hence,

$$f_1^i = 0, \quad f_2 = 0, \quad f_3^i = F(t)\, \delta(x_1,x_2,x_3-x_3^{(S)}), \tag{3.3}$$

$$q^i = Q(t)\, \delta(x_1,x_2,x_3-x_3^{(S)}), \tag{3.4}$$

where the source-strength $\{F(t),Q(t)\}$ is understood to be zero when $t < 0$.

In the analysis of the solution of Eqs. (3.1) - (3.4), we take advantage of the invariance of the configuration with respect to time and with respect to the horizontal coordinates.

4. TRANSFORMED WAVE EQUATIONS

Using the one-sided Laplace transform with respect to time

$$\hat{f}(x_1,x_2,x_3,s) = \int_0^\infty f(x_1,x_2,x_3,t)\, \exp(-st)\, dt, \quad \mathrm{Re}(s) > 0, \tag{4.1}$$

and subsequently a Fourier transform with respect to the horizontal coordinates

$$\tilde{f}(\alpha_1,\alpha_2,x_3,s) = \int_{-\infty}^{\infty} dx_2 \int_{-\infty}^{\infty} \hat{f}(x_1,x_2,x_3,s)\, \exp[is(\alpha_1 x_1+\alpha_2 x_2)]\, dx_1 \tag{4.2}$$

with the inverse Fourier transform

$$\hat{f}(x_1,x_2,x_3,s) = \left(\frac{s}{2\pi}\right)^2 \int_{-\infty}^{\infty} d\alpha_2 \int_{-\infty}^{\infty} \tilde{f}(\alpha_1,\alpha_2,x_3,s)\, \exp[-is(\alpha_1 x_1+\alpha_2 x_2)]\, d\alpha_1, \tag{4.3}$$

lead to the transformed acoustic wave equations for the fundamental acoustic quantities $\tilde{p}$ and $\tilde{v}_3$

$$\partial_3 \tilde{p} + s\,\rho\,\tilde{v}_3 = \tilde{f}_3^i, \tag{4.4}$$

$$\partial_3 \tilde{v}_3 + s\,\gamma^2 \rho^{-1}\,\tilde{p} = \tilde{q}^i, \tag{4.5}$$

in which $\gamma = \gamma(x_3)$ is the vertical slowness given as

$$\gamma = (c^{-2} + \alpha_1^2 + \alpha_2^2)^{1/2} > 0, \tag{4.6}$$

and $c = c(x_3)$ is the acoustic wave speed. In our transformed equations, the source distributions are the "force"

$$\tilde{f}_3^i = \hat{F}_3(s)\ \delta(x_3 - x_3^{(S)}), \tag{4.7}$$

and the "volume injection"

$$\tilde{q}^i = \hat{Q}(s)\ \delta(x_3 - x_3^{(S)}). \tag{4.8}$$

In the next sections we consider some approximate methods to solve our transformed acoustic wave equations in the layered configuration at hand.

5. CONTRAST SOURCES IN A BACKGROUND MEDIUM

We first observe that the total field $\{\tilde{p}, \tilde{v}_3\}$ can be written as the sum of two field constituents:

$$\tilde{p} = \tilde{p}^i + \tilde{p}^s, \quad \tilde{v}_3 = \tilde{v}_3^i + \tilde{v}_3^s, \tag{5.1}$$

where $\{\tilde{p}^i, \tilde{v}_3^i\}$ are the transformed quantities of the incident field in the (in)homogeneous background medium with $\rho_B(x_3)$, $\kappa_B(x_3)$, and where $\{\tilde{p}^s, \tilde{v}_3^s\}$ denote the transformed quantities of the scattered field. The incident field satisfies the equations

$$\partial_3 \bar{p}^i + s\,\rho_B\,\bar{v}_3^i = \bar{f}_3^i, \tag{5.2}$$

$$\partial_3 \bar{v}_3^i + s\,\gamma_B^2\rho_B^{-1}\,\bar{p}^i = \bar{q}^i, \tag{5.3}$$

where $\gamma_B = \gamma_B(x_3)$ is the vertical slowness in the background medium, given as

$$\gamma_B = (c_B^{-2} + \alpha_1^2 + \alpha_2^2)^{1/2} > 0, \tag{5.4}$$

and $c_B = c_B(x_3)$ is the wave speed in the background medium is. When the total field satisfies Eqs. (4.4) - (4.5), the scattered field satisfies the equations

$$\partial_3 \bar{p}^s + s\,\rho_B\,\bar{v}_3^s = -\bar{f}_3, \tag{5.5}$$

$$\partial_3 \bar{v}_3^s + s\,\gamma_B^2\rho_B^{-1}\,\bar{p}^s = \bar{q}^s, \tag{5.6}$$

in which the scattered field is understood to be excited in the background medium by the contrast source distributions

$$\bar{f}_3^s = -s\,(\rho - \rho_B)\,\bar{v}_3, \tag{5.7}$$

$$\bar{q}^s = -s\,(\gamma^2\rho^{-1} - \gamma_B^2\rho_B^{-1})\,\bar{p}. \tag{5.8}$$

Note that in the expressions for the contrast source distributions of Eqs. (5.7) and (5.8) the total field quantities $\bar{p}$ and $\bar{v}_k$ occur. From Eqs. (5.5) and (5.6), the scattered acoustic pressure is obtained as

$$\bar{p}^s(x_3) = \int_{-\infty}^{\infty} \bar{f}_3^s(x_3') \, \bar{p}^f(x_3,x_3') \, dx_3' + \int_{-\infty}^{\infty} \bar{q}^s(x_3') \, \bar{p}^q(x_3,x_3') \, dx_3', \tag{5.9}$$

$$\bar{v}_3^s(x_3) = \int_{-\infty}^{\infty} \bar{f}_3^s(x_3') \, \bar{v}_3^f(x_3,x_3') \, dx_3' + \int_{-\infty}^{\infty} \bar{q}^s(x_3') \, \bar{v}_3^q(x_3,x_3') \, dx_3', \tag{5.10}$$

where $\{\bar{p}^f,\bar{v}_3^f\}$ is the acoustic wave field excited by a unit force in the x_3-direction at $x_3 = x_3'$ and $\{\bar{p}^q,\bar{v}_3^q\}$ is the acoustic wave field excited by a unit volume injection source at $x_3 = x_3'$. These unit source fields satisfy the equations

$$\partial_3 \bar{p}^f + s \, \rho_B \, \bar{v}_3^f = \delta(x_3-x_3'), \tag{5.11}$$

$$\partial_3 \bar{v}_3^f + s \, \gamma_B^2 \rho_B^{-1} \, \bar{p}^f = 0, \tag{5.12}$$

and

$$\partial_3 \bar{p}^q + s \, \rho_B \, \bar{v}_3^q = 0, \tag{5.13}$$

$$\partial_3 \bar{v}_3^q + s \, \gamma_B^2 \rho_B^{-1} \, \bar{p}^q = \delta(x_3-x_3'). \tag{5.14}$$

So far we deal with a rigorous analysis. As soon as the unit source solutions $\{\bar{p}^i,\bar{v}_3^i\}$ of Eqs. (5.2) - (5.3), $\{\bar{p}^f,\bar{v}_3^f\}$ of Eqs. (5.11) - (5.12), and $\{\bar{p}^q,\bar{v}_3^q\}$ of Eqs. (5.13) - (5.14) are calculated, we can take the total field in Eqs. (5.7) - (5.8) to be the incident field and calculate the scattered field from Eqs. (5.9) - (5.10). This procedure is known as the Born approximation.

6. FIRST BORN APPROXIMATION

In the First Born approximation we take the background medium to be the homogeneous medium, i.e.

$$\rho_B = \rho_0, \quad c_B = c_0. \tag{6.1}$$

The incident field $\{\bar{p}^i, \bar{v}_3^i\}$ in this homogeneous background medium is obtained as

$$\bar{p}^i(x_3) = (2\gamma_0)^{-1}[\gamma_0\hat{F} + \rho_0\hat{Q}] \exp[-s\gamma_0(x_3 - x_3^{(S)})], \tag{6.2}$$

$$\bar{v}_3^i(x_3) = (\gamma_0/\rho_0)\, \bar{p}^i(x_3), \tag{6.3}$$

when $x_3 > x_3^{(S)}$,

and the unit-source solutions $\{\bar{p}^f, \bar{v}_3^f\}$ and $\{\bar{p}^q, \bar{v}_3^q\}$ with source location at $x_3 = x_3'$ and observer location at $x_3 = x_3^{(R)}$ as

$$\bar{p}^f(x_3^{(R)}, x_3') = -(1/2) \exp[s\gamma_0(x_3^{(R)} - x_3')], \tag{6.4}$$

$$\bar{v}_3^f(x_3^{(R)}, x_3') = -(\gamma_0/\rho_0)\, \bar{p}^f(x_3^{(R)}, x_3'), \tag{6.5}$$

$$\bar{p}^q(x_3^{(R)}, x_3') = (\rho_0/2\gamma_0) \exp[s\gamma_0(x_3^{(R)} - x_3')], \tag{6.6}$$

$$\bar{v}_3^q(x_3^{(R)}, x_3') = -(\gamma_0/\rho_0)\, \bar{p}^f(x_3^{(R)}, x_3'), \tag{6.7}$$

when $x_3^{(R)} < x_3'$.

Subsequently, we take in the contrast source distributions of Eqs. (5.7) - (5.8) the total field to be equal to the incident field. This approximation is valid for small values of $\rho - \rho_0$ and $c^{-2} - c_0^{-2}$ only. We then have

$$\tilde{p}^s(x_3^{(R)}) = \frac{s}{4} \int_{x_3^{(0)}}^{\infty} (\gamma_0 \hat{F} + \rho_0 \hat{Q}) \frac{\gamma_0^2 \rho_0^{-1} \rho - \gamma^2 \rho^{-1} \rho_0}{\gamma_0^2} \exp[-s\gamma_0 z)] \, dx_3', \tag{6.8}$$

$$\tilde{v}_3^s(x_3^{(R)}) = \frac{s}{4} \int_{x_3^{(0)}}^{\infty} (\gamma_0 \rho_0^{-1} \hat{F} + \hat{Q}) \frac{\gamma_0^2 \rho_0^{-1} \rho - \gamma^2 \rho^{-1} \rho_0}{\gamma_0} \exp[-s\gamma_0 z)] \, dx_3', \tag{6.9}$$

in which $\gamma_0 = (c_0^{-2} + \alpha_1^2 + \alpha_2^2)^{1/2}$ and the vertical travel distance $z = z(x_3')$ between receiver and source via the reflection point x_3' is given by

$$z = 2x_3' - x_3^{(R)} - x_3^{(S)}. \tag{6.10}$$

Note that the integrals start at $x_3^{(0)}$, since the actual medium is identical to the background medium for values of x_3 less than $x_3^{(0)}$.

7. SPACE-TIME DOMAIN RESULTS FOR A VOLUME INJECTION SOURCE

In the following, we only consider the point source of the volume injection type, i.e. $F = 0$, $Q = 0$. This type of source is of importance in marine seismics. We then measure the pressure p only. We therefore continue our analysis with Eq. (6.8). For our configuration at hand (Fig. 1), the integral of Eq. (6.8) can be calculated analytically. We then obtain

$$(\frac{s}{2\pi})^2 \tilde{p}^s(\alpha_1, \alpha_2, x_3^{(R)}, s) = \rho_0 \, s^2 \, \hat{Q}(s) \, \tilde{G}(\alpha_1, \alpha_2, x_3^{(R)}, s), \tag{7.1}$$

in which the spectral representation of Green's function $\bar{G} = \bar{G}(\alpha_1,\alpha_2,x_3^{(R)},s)$ is given by contributions of the interfaces $x_3 = x_3^{(n)}$, n=0,1,2,...,N, as

$$\bar{G} = \frac{1}{8\pi^2}\sum_{n=0}^{N}\left[A_n + \frac{B_n}{4\gamma_0^2}\right]\frac{\exp[-s\gamma_0 z_n]}{\gamma_0}, \tag{7.2}$$

with

$$z_n = z(x_3^{(n)}) = 2x_3^{(n)} - x_3^{(R)} - x_3^{(S)}, \tag{7.3}$$

while A_n and B_n are given by

$$A_n = \tfrac{1}{4}(\rho_{n+1}\rho_0^{-1} - \rho_0\rho_{n+1}^{-1}) - \tfrac{1}{4}(\rho_n\rho_0^{-1} - \rho_0\rho_n^{-1}) = \frac{\rho_{n+1} - \rho_n}{\rho_{n+1} + \rho_n} \tag{7.4}$$

and

$$B_n = (c_n^{-2} - c_0^{-2})\rho_0\rho_n^{-1} - (c_{n+1}^{-2} - c_0^{-2})\rho_0\rho_{n+1}^{-1} = c_n^{-2} - c_{n+1}^{-2}. \tag{7.5}$$

The approximations made in Eqs. (7.4) and (7.5) are consistent with the low-contrast approximations of the Born approximation. Note that the term $A_n + B_n(2\gamma_0)^{-2}$ in Eq. (7.2) is the low-contrast approximation of the reflection factor of an acoustic wave in our transform domain. This reflection factor with respect to an interface at $x_3^{(n)}$ is given by

$$r_n = \frac{\gamma_n\rho_n^{-1} - \gamma_{n+1}\rho_{n+1}^{-1}}{\gamma_n\rho_n^{-1} + \gamma_{n+1}\rho_{n+1}^{-1}}, \tag{7.6}$$

in which

$$\gamma_n = (c_n^{-2} + \alpha_1^2 + \alpha_2^2)^{1/2} = \gamma_0 \left(1 + \frac{c_n^{-2} - c_0^{-2}}{\gamma_0^2}\right)^{1/2} = \gamma_0 \left(1 + \frac{c_n^{-2} - c_0^{-2}}{2\gamma_0^2}\right). \tag{7.7}$$

In the last expression of Eq. (7.7), we have used a low-contrast approximation. Using this approximation in the expression for the reflection factor, we obtain the low-contrast approximation for the reflection factor as

$$r_n = \frac{\rho_{n+1} - \rho_n}{\rho_{n+1} + \rho_n} + \frac{c_n^{-2} - c_{n+1}^{-2}}{4\gamma_0^2} = A_n + \frac{B_n}{4\gamma_0^2}. \tag{7.8}$$

From Eqs. (7.2) and (7.8), we observe the well-known feature that the first Born approximation takes into account the primary reflections only. Further, we remark that the approximation of the reflection factor given by Eq. (7.8) is only valid when γ_{n+1} is a regular function of α and β. This excludes the possibility of head-wave occurence. The latter waves only occur for large offsets, restricting the admissible values of r. This is again consistent with the Born approximation.

Under these restrictions, solutions in the time-space domain are directly obtained with the aid of Cagniard-De Hoop technique (De Hoop 1960, Aki and Richards 1980, p. 224). Applying this technique, we have

$$\int_{-\infty}^{\infty} d\alpha_2 \int_{-\infty}^{\infty} \frac{\exp[-s\gamma_0 z_n]}{2\pi\,\gamma_0} \exp[-is(\alpha_1 x_1 + \alpha_2 x_2)]\, d\alpha_1 = \int_{R_n/c_0}^{\infty} \frac{\exp(-st)}{R_n}\, dt, \tag{7.9}$$

and

$$\int_{-\infty}^{\infty} d\alpha_2 \int_{-\infty}^{\infty} \frac{\exp[-s\gamma_0 z_n]}{2\pi\ \gamma_0^3} \exp[-is(\alpha_1 x_1 + \alpha_2 x_2)]\ d\alpha_1$$

$$= \int_{R_n/c_0}^{\infty} \frac{z_n\ t\ \exp(-st)}{(t^2 - r^2/c_0^2)^{3/2}}\ dt, \tag{7.10}$$

in which the horizontal offset r between receiver and source is defined as

$$r = [(x_1^{(R)})^2 + (x_2^{(R)})^2]^{1/2} > 0 \tag{7.11}$$

and the travel distance R_n between receiver and source via the reflection point $x_3^{(n)}$ as

$$R_n = [r^2 + z_n^2]^{1/2} > 0. \tag{7.12}$$

The time-domain representation of the scattered field p^s is then recognized as

$$p^s(r, x_3^{(R)}, t) = \rho_0\ \partial_t^2 (Q(t) * G(r, x_3^{(R)}, t)), \tag{7.13}$$

in which * denotes the convolution and the space-time Green's function $G = G(r, x_3^{(R)}, t)$ denotes the impulse response of the system and is given by

$$G = \frac{1}{4\pi} \sum_{n=0}^{N} \left[\frac{A_n}{R_n} + \frac{B_n\ z_n\ t}{4(t^2 - r^2/c_0^2)^{3/2}}\right] H(t - R_n/c_0), \tag{7.14}$$

where H is the unit step function defined by

$$H(t) \begin{cases} = 1, & t > 0, \\ = 0, & t < 0. \end{cases} \tag{7.15}$$

Now, we shall present some numerical results for the nine-layer configuration of Table 1. For this configuration, Drijkonigen and Fokkema (1987) have computed the Green's function of Eq. (7.14) by using the exact Cagniard-De Hoop technique with only primary reflections. We shall compare our approximate results with the ones obtained from this Cagniard-De Hoop technique. In Fig. 2, we present the results of the First Born approximation for two different values of the offset r. The dashed lines represent the exact results of the Cagniard-De Hoop technique with primaries only. We observe that the results of the Born approximation do not fit the arrival times very well.

8. RMS BORN APPROXIMATION

In order to improve the Born approximation, we should use a more realistic background medium. The disadvantage of using a more realistic background medium is the complication of the field solution. Therefore, we avoid the precise assumption of a realistic background medium. As starting point, we have the solution of the Cagniard-De Hoop technique with primary reflections only. The Green's function is obtained as (Drijkonigen and Fokkema 1987)

$$\tilde{G} = \frac{1}{8\pi^2} \sum_{n=0}^{N} \Gamma_n \frac{\exp[-s \sum_{m=0}^{n} \gamma_m h_m]}{\gamma_0} , \tag{8.1}$$

in which the reflection factor Γ_n is given by Eq. (7.6) and where h_m denotes the vertical wave path that the acoustic wave has traversed in the layer with wave speed c_m. Note that in Eq. (8.1), we have taken the transmission factors of all interfaces equal to 1. This approximation is consistent with

the low-contrast approximations. The total vertical geometric path is given by

$$z_n = \Sigma_{m=0}^{n} h_m, \tag{8.2}$$

where

$$h_0 = 2x_3^{(0)} - x_3^{(R)} - x_3^{(S)},$$

$$h_m = 2(x_3^{(m)} - x_3^{(m-1)}), \quad m = 1, 2, 3, \ldots . \tag{8.3}$$

Further, we have an upper bound and a lower bound for the vertical wave propagation term $\Sigma_m \gamma_m h_m$. For real α_1 and α_2, we are able to write (Van den Berg and Fokkema 1987)

$$(c_n'^{-2}+\alpha_1^2+\alpha_2^2)^{1/2} z_n \leq \Sigma_{m=0}^{n} \gamma_m h_m \leq (c_n''^{-2}+\alpha_1^2+\alpha_2^2)^{1/2} z_n, \tag{8.4}$$

where c_n' is the root-mean square wave speed defined as

$$c_n' = (\Sigma_{m=0}^{n} c_m h_m)^{1/2} / (\Sigma_{m=0}^{n} c_m^{-1} h_m)^{1/2} \tag{8.5}$$

and c_n'' is the root-mean square wave speed defined as

$$c_n'' = (\Sigma_{m=0}^{n} h_m)^{1/2} / (\Sigma_{m=0}^{n} c_m^{-2} h_m)^{1/2}. \tag{8.6}$$

Note that only the first definition of Eq. (8.5) for the root-mean-square wave speed is commonly used in seismics (Cf. Helbig 1981, p. 159) to replace a stack of layers by a single layer with some replacement velocity. From

(8.4) it is obvious that a very good approximation for the vertical wave propagation is given by

$$\Sigma_{m=0}^{n} \gamma_m h_m = \gamma_n^{rms} z_n, \tag{8.7}$$

with

$$\gamma_n^{rms} = [(c_n^{rms})^{-2} + \alpha_1^2 + \alpha_2^2]^{1/2} \tag{8.8}$$

and

$$c_n^{rms} = (c_n' c_n'')^{1/2}. \tag{8.9}$$

Using the result of Eq. (8.7) in our expression of the Green's function of Eq. (8.1), we obtain

$$\bar{G} = \frac{1}{8\pi^2} \Sigma_{n=0}^{N} \Gamma_n \frac{\exp[-s \gamma_n^{rms} z_n]}{\gamma_0}. \tag{8.10}$$

At the interface at $x_3^{(n)}$, in the same way as in Eq. (7.7), we write

$$\gamma_n = (c_n^{-2} + \alpha_1^2 + \alpha_2^2)^{1/2} = \gamma_n^{rms} \left(1 + \frac{c_n^{-2} - (c_n^{rms})^{-2}}{(\gamma_n^{rms})^2}\right)^{1/2}$$

$$= \gamma_n^{rms} \left(1 + \frac{c_n^{-2} - (c_n^{rms})^{-2}}{2(\gamma_n^{rms})^2}\right) \tag{8.11}$$

and in the same way we write γ_{n+1} as

$$\gamma_{n+1} \approx \gamma_n^{rms} \left(1 + \frac{c_{n+1}^{-2} - (c_n^{rms})^{-2}}{2(\gamma_n^{rms})^2}\right). \tag{8.12}$$

Hence, the low-contrast approximation of the reflection factor is obtained as

$$\Gamma_n = \frac{\rho_{n+1} - \rho_n}{\rho_{n+1} + \rho_n} + \frac{c_n^2 - c_{n+1}^2}{4(\gamma_n^{rms})^2} = A_n + \frac{B_n}{(2\gamma_n^{rms})^2}. \tag{8.13}$$

For the validity of Eq. (8.13) and the following analysis, we refer to the remarks made below Eq. (7.8). With $\gamma_0 = \gamma_n^{rms}$ at the interface $x_3^{(n)}$ and the low-contrast result of Eq. (8.13), the low-contrast approximation of the Green's function of Eq. (8.10) is arrived at

$$\tilde{G} = \frac{1}{8\pi^2} \sum_{n=0}^{N} \left[A_n + \frac{B_n}{4(\gamma_n^{rms})^2}\right] \frac{\exp[-s\,\gamma_n^{rms}\,z_n]}{\gamma_n^{rms}}. \tag{8.14}$$

Using the results of Eqs. (7.9) and (7.10), with γ_0 replaced by γ_n^{rms}, the space-time Green's function is obtained as

$$G = \frac{1}{4\pi} \sum_{n=0}^{N} \left[\frac{A_n}{R_n} + \frac{B_n\, z_n\, t}{4(t^2-(r/c_n^{rms})^2)^{3/2}}\right] H(t-R_n/c_n^{rms}), \tag{8.15}$$

Note that the travel time

$$T_n = R_n / c_n^{rms} \tag{8.16}$$

is our approximation of the exact travel time. Further, in the denominator of the second term in Eq. (8.11), we may replace c_n^{rms} by c_0. This is consistent with our approximations already made. We finally end up with

$$G(t) = \frac{1}{4\pi} \sum_{n=0}^{N} \left[\frac{A_n}{R_n} + \frac{1}{4} B_n z_n w(t)\right] H(t-T_n), \tag{8.17}$$

where

$$A_n = (\rho_{n+1} - \rho_n) / (\rho_{n+1} + \rho_n) \tag{8.18}$$

and

$$B_n = c_n^{-2} - c_{n+1}^{-2}, \tag{8.19}$$

$$w(t) = t / (t^2 - r^2/c_0^2)^{3/2}. \tag{8.20}$$

If, in the expression of the travel times of Eq.(8.16), we enforce c_n^{rms} to be equal to c_0, we obtain the space-time Green's function of the First Born approximation with the homogeneous background of Section 7. The result of Eq. (8.17) can be interpreted as some distorted-wave Born approximation using some background medium with our chosen vertical varying root-mean-square acoustic wave speed.

We subsequently present some numerical results for our nine-layer configuration of Table 1. We compare our approximate results with the ones obtained from the Cagniard-De Hoop technique. In Fig. 3, the dashed lines represent the exact results of the Cagniard-De Hoop technique with primaries only. We observe that the results of our simple expression of the RMS Born approximation are in good agreement with the much more complicated Cagniard-De Hoop technique for primaries only.

9. VELOCITY INVERSION

We first consider the simplified case that there is no contrast in mass density, i.e. $\rho_n = \rho_0$, for all n. In order to obtain the Green's function G(t), the inversion procedure consists of a deconvolution of the data with the known source signature. For $t > r/c_0$, we divide the obtained values by w(t). Then, we determine the location of the jumps in the curve G(t)/w(t). These time instants are the arrival times T_n, n=0,1,2,...,N-1. The last time instant considered in the data is defined as T_N.

With the results of Eq. (8.17) and $A_n = 0$, for all n, the values of the wave speed are obtained from

$$c_{n+1}^{-2} = c_n^{-2} - B_n, \quad n = 0, 1, \ldots, N-1, \tag{9.1}$$

where B_n is obtained from the recurrence relations

$$B_n z_n = \frac{16}{T_{n+1} - T_n} \int_{T_n}^{T_{n+1}} G(t)/w(t)\, dt - \sum_{m=0}^{n-1} B_m z_m, \tag{9.2}$$

$$z_n = (R_n^2 - r^2)^{1/2}. \tag{9.3}$$

$$R_n = T_n c_n^{rms}, \tag{9.4}$$

The time integral of Eq. (9.2) is computed numerically by a simple rectangular integration rule over the discrete time samples. The RMS-velocity is determined recursively as

$$c_n^{rms} = (c_n' c_n'')^{1/2}, \tag{9.5}$$

with

$$c_n' = (\Sigma_{m=0}^{n} c_m(T_m-T_{m-1}))^{1/2} / (\Sigma_{m=0}^{n} c_m^{-1}(T_m-T_{m-1}))^{1/2} \tag{9.6}$$

and

$$c_n'' = (\Sigma_{m=0}^{n} (T_m-T_{m-1}))^{1/2} / (\Sigma_{m=0}^{n} c_m^{-2}(T_m-T_{m-1}))^{1/2}, \tag{9.7}$$

in which

$$T_{-1} = r/c_0. \tag{9.8}$$

Note that these definitions of c_n' and c_n'' differ from Eqs. (8.5) and (8.6), but it has been verified numerically that the final results for c_n^{rms} do not differ significantly. The present definitions are more advantageous in the inverse scheme, since we only can determine the arrival times from the data. As soon we have determined c_n^{rms}, the precise locations of z_n (and hence h_n) are obtained as a result. In this way a very simple inversion scheme is arrived at.

In Fig. 4, we present the synthetic data of the Cagniard-De Hoop method (with primaries only) of the Green's function for the configuration of Table 1, provided there is no mass-density contrast. In the same figure, we also present the results of the function $G(t)/w(t)$, when $t > r/c_0$. Using these data, the reconstructed wave speeds are presented in Fig. 5. A very close agreement with the exact results (dashed line) is observed. In view of the simplicity of the inversion procedure, we have arrived at a very elegant single-pass seismic inversion scheme.

10. COMPLETE INVERSION

We now consider the complete inversion scheme. We observe that the expression of G(t) of Eq. (8.17) consists of two constituents, where the first one contains mass-density information and the second one contains velocity information. When there is mass-density contrast we have to modify our inversion scheme as follows. We first determine the jumps in the curve of G(t). These time instants are the arrival times T_n, n=0,1,2,...,N-1. The last time interval considered in the data is defined as T_N. In each time interval $T_{n+1} < t < T_n$, n=0,1,2,...,N-1, we then perform a simple least-square-error fit of the right-hand side of Eq. (8.17) to the data. Then, the values of $\sum_{m=0}^{n} A_m/R_m$ and $\sum_{m=0}^{n} \frac{1}{4}B_m z_m$ are determined from the minimization procedure of the quantities

$$\int_{T_n}^{T_{n+1}} \left|4\pi\, G(t) - \sum_{m=0}^{n} A_m/R_m - \left(\sum_{m=0}^{n} \tfrac{1}{4}B_m z_m\right) w(t)\right|^2 dt.$$

The values of the mass density and the wave speed are then obtained as

$$\rho_{n+1} = \rho_n\,(1+A_n)/(1-A_n), \tag{10.1}$$

$$c_{n+1}^{-2} = c_n^{-2} - B_n, \tag{10.2}$$

where A_n and B_n are obtained from the recurrence relations

$$A_n/R_n = 4\pi\,\frac{a_{22}b_1 - a_{12}b_2}{a_{11}\,a_{22} - a_{22}^2} - \sum_{m=0}^{n-1} A_m/R_m, \tag{10.3}$$

$$B_n z_n = 16\pi \frac{a_{11}b_2 - a_{12}b_1}{a_{11}a_{22} - a_{22}^2} - \sum_{m=0}^{n-1} B_m z_m, \tag{10.4}$$

in which

$$a_{11} = \int_{T_n}^{T_{n+1}} dt, \tag{10.5}$$

$$a_{12} = \int_{T_n}^{T_{n+1}} w(t)\, dt, \tag{10.6}$$

$$a_{22} = \int_{T_n}^{T_{n+1}} w^2(t)\, dt, \tag{10.7}$$

$$b_1 = \int_{T_n}^{T_{n+1}} G(t)\, dt, \tag{10.8}$$

$$b_2 = \int_{T_n}^{T_{n+1}} G(t)\, w(t)\, dt. \tag{10.9}$$

The integrals of Eqs. (10.8) and (10.9) have to be calculated numerically, using e.g. a rectangular integration rule over the time samples. The integrals of Eqs. (10.5) - (10.7) can be calculated analytically. However, it is more consistent to evaluate this integrals numerically in the same manner as the other ones.

Without any changes, the values of z_n, R_n and c_n^{rms} follow from Eqs. (9.3) - (9.8) of the previous section. This concludes our complete inversion scheme. In contrast to Raz (1981a), we are able to reconstruct within our approximations both the density and the velocity profile. The only a priori information we have used is the knowledge that the horizontally stratified

medium consists of a stack of homogeneous layers. This assumption complies with the presence of jumps in the data corresponding to the arrival times T_n of the reflected waves from the interfaces.

In Fig. 6, the reconstructed mass-density profile and the wave speed profile are shown. As starting point, we have taken the synthetic data of Fig. 3, when the offset between source and receiver is equal to 50 m. In Fig. 6, the exact profiles are presented as the dashed lines. The reconstructed mass-density profile is in close agreemert with the exact one. The reconstructed wave speed profile differs more from the exact one. The reason is that the second term of Eq. (8.17) with the velocity contrast is substantially less than the first term with the density contrast. Hence, small errors in the reconstructed mass density has a great influence on the reconstructed wave speeds. To illustrate this effect, we apply our complete inversion scheme to the synthetic data of Fig. 4. These are the data of the configuration without any contrast in mass density. The reconstructed profiles are shown in Fig. 7. The inverted mass density indeed approximates the constant mass density $\rho_0 = 1000$ very well. But the small discrepancies in this curve are sufficient to yield an inverted wave speed profile deviating more from the exact result than the one of Fig. 5. In Fig. 5, we have used the a priori information that there is no density contrast.

11. CONCLUSIONS

We have derived a simple closed-form expression for the space-time domain scattered field in a layered structure. The results of the forward modeling are in good agreement with the synthetic data of the Cagniard-De Hoop technique for primaries only. Our closed-form expression consists of two constituents; in the first one only the mass-density contrast occurs, while

in the second one only the velocity contrast is present. Using a single trace, both the mass densities and the wave speeds of the layered structure can be reconstructed from synthetic data. The inversion operator based on our RMS Born approximation is a local operator. The inversion is performed while marching on in time. The inversion process is of the order of a few seconds on a IBM Personal Computer AT. Future research will be concentrated on applying the RMS Born inverse operator to real data. Then, multiple offsets of source and receiver are needed to cope with noisy data.

ACKNOWLEDGMENTS

The authors wish to thank Professor A.T. de Hoop for useful discussions concerning the Born approximation and the Cagniard-De Hoop method.
The first author has partially performed the research of this paper while he was a visiting professor of the Universidade Federal da Bahia, Brazil, under the responsibility of the Programa de Pesquisa e Pós-Graduação en Geophisica da Universidada Federal da Bahia - PPPG/UFBA supported by Petrobras and CNPq. This support is greatfully acknowledged.

REFERENCES

AKI, K. and RICHARDS, P.G. 1980. Body waves in media with depth-dependent properties, in Quantitative Seismology I, chapter 9, W.H. Freeman.

BEYLKIN, G., and ORISTAGLIO, M.L. 1985. Distorted-wave Born and distorted wave Rytov approximations, Optics Communications 53, 213-216.

BLEISTEIN, N., and GRAY, S.H. 1985. An extension of the Born inversion method to a depth dependent reference profile, Geophysical Prospecting 33, 999-1022.

CLAYTON, R.W., and STOLT, R.H. 1981. A Born-WKBJ inversion method for acoustic reflection data, Geophysics 46, 1559-1567.

COHEN, J.K., and BLEISTEIN, N. 1977. An inverse method for determining small variations in propagation speed, SIAM J. of Appl. Math. 32, 784-799.

COHEN, J.K., and BLEISTEIN, N. 1979. Velocity inversion procedure for acoustic waves, Geophysics 44, 1077-1087.

DE HOOP, A.T. 1960, A modification of Cagniard's method for solving seismic pulse problems, Applied Scientific Research, Section B8, 349-356.

DRIJKONINGEN, G.G. and FOKKEMA, J.T. 1987, The exact seismic response of an ocean and a N-layer configuration, Geophysical Prospecting 35, 33-61.

FOSTER, D.J., and CARRION, Ph.M. 1984, Born inversion with a variable background velocity, Geophysics 49, 1794-1797.

HELBIG, K. 1981, Ray geometric migration in seismic prospecting, in The solution of the inverse problem in geophysical prospecting, R. Cassinis, Ed., Plenum Press, 141-177.

PHINNEY, R., and FRAZER, L.N. 1978. On the theory of seismic imaging by Fourier transform. Presented at the 48th Annual International SEG Meeting, October 31, in San Francisco.

RAZ, S. 1981a. Direct reconstruction of velocity and density profiles for scattered field data, Geophysics 46, 832-836.

RAZ, S. 1981b. Three-dimensional velocity profile inversion from finite offset data, Geophysics 46, 837-842.

VAN DEN BERG, P.M., and FOKKEMA, J.T. 1988, A RMS-approximation in the Cagniard-De Hoop method, to be published.

WEGLEIN, A.B., VIOLETTE, P.B., and KEHO , T.H. 1986, Using multiparameter Born theory to obtain certain exact multiparameter inversion goals, Geophysics 51, 1069 -1074.

LIST OF CAPTIONS

Fig. 1. Description of the configuration.

Table 1. The location of the interfaces, mass density and wave speed of the layers for the nine-layer configuration.

Fig. 2. The First Born approximation of the space-time Green's function for the nine-layer configuration of Table 1; $x_3^{(S)} = x_3^{(R)} = 7.5$ m and r = 100 m and r = 50 m, respectively.

Fig. 3. The RMS Born approximation of the space-time Green's function for the nine-layer configuration of Table 1; $x_3^{(S)} = x_3^{(R)} = 7.5$ m and r = 100 m and r = 50 m, respectively.

Fig. 4. The results of the space-time Green's function G and G/w for the nine-layer configuration of Table 1, provided $\rho_n = \rho_0$, all n, while $x_3^{(S)} = x_3^{(R)} = 7.5$ m and r = 50 m.

Fig. 5. Reconstructed wave speed c_n from the data of Fig. 4.

Fig. 6. Reconstructed mass density ρ_n and wave speed c_n from the data of Fig. 3, when r = 50 m.

Fig. 7. Reconstructed mass density ρ_n and wave speed c_n from the data of Fig. 4.

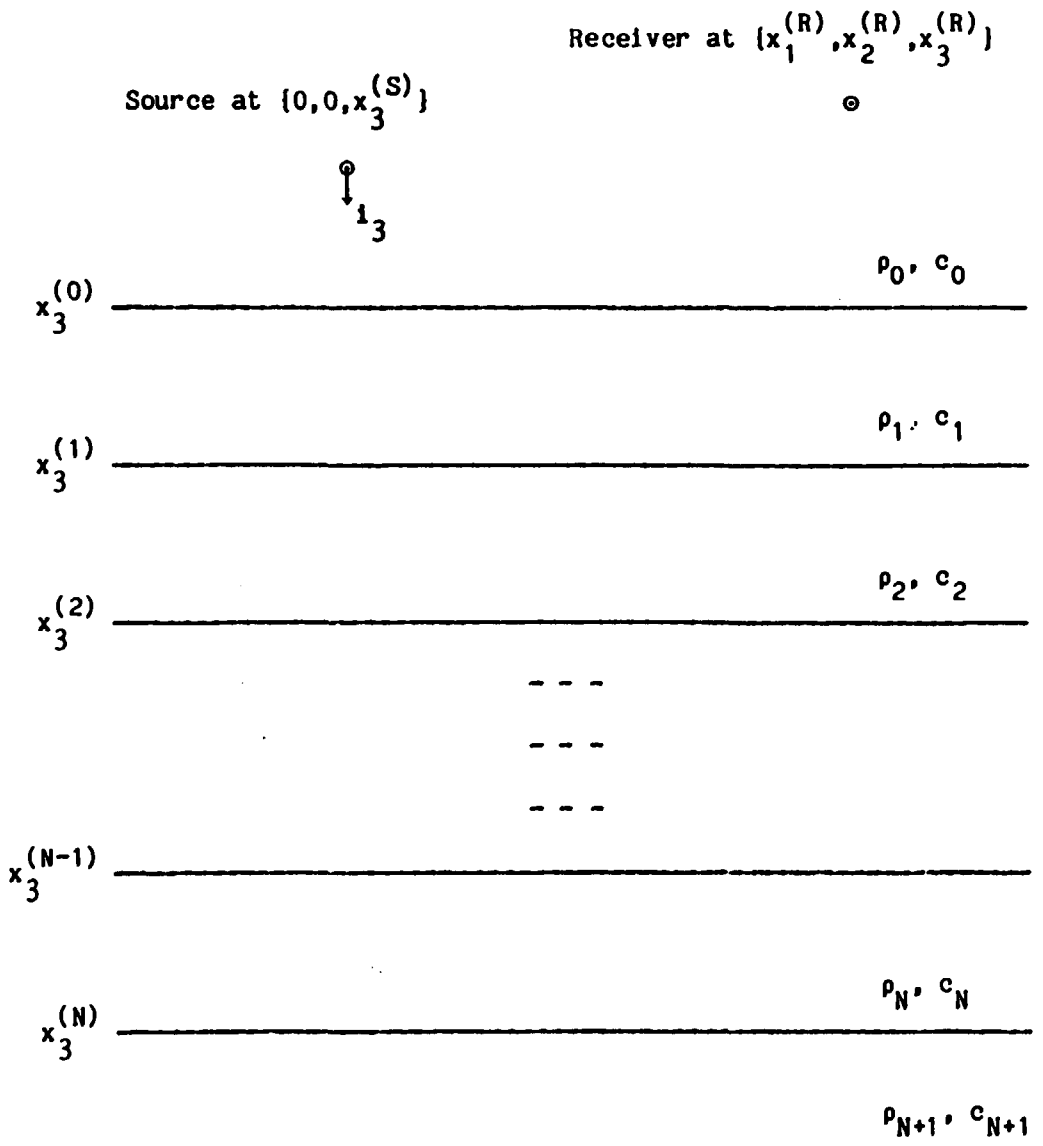

Fig. 1. Description of the configuration.

Table 1. The location of the interfaces, mass density and wave speed of the layers for the nine-layer configuration.

n	$x_3^{(n)}$ (m)	ρ_n (kg/m^3)	c_n (m/s)
0	70	1000	1500
1	100	1010	1600
2	135	1200	1700
3	175	1200	1800
4	210	1250	1700
5	260	1150	1600
6	340	1200	1900
7	415	1300	2000
8	-	1500	2200

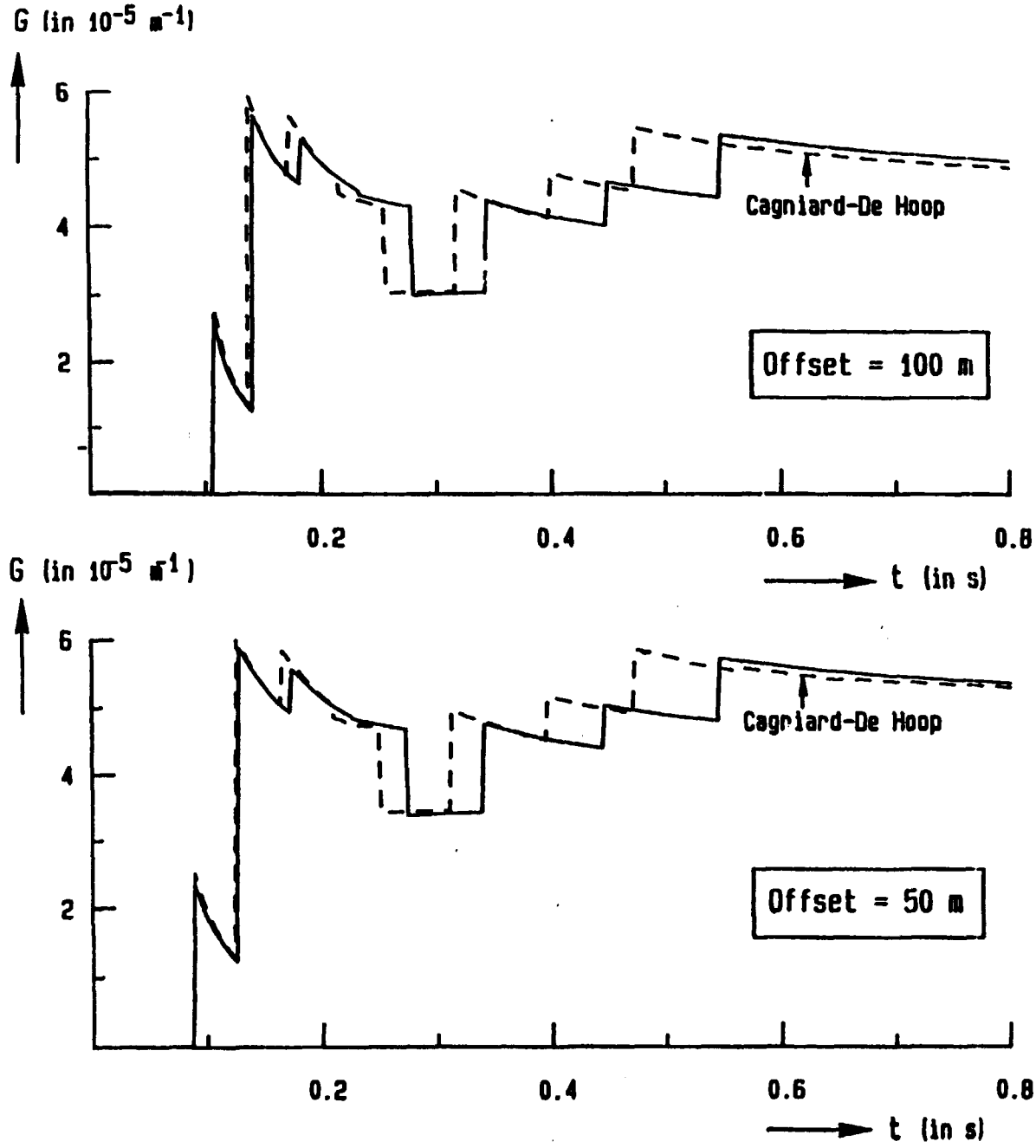

Fig. 2. The First Born approximation of the space-time Green's function for the nine-layer configuration of Table 1; $x_3^{(S)} = x_3^{(R)} = 7.5$ m and r = 100 m and r = 50 m, respectively.

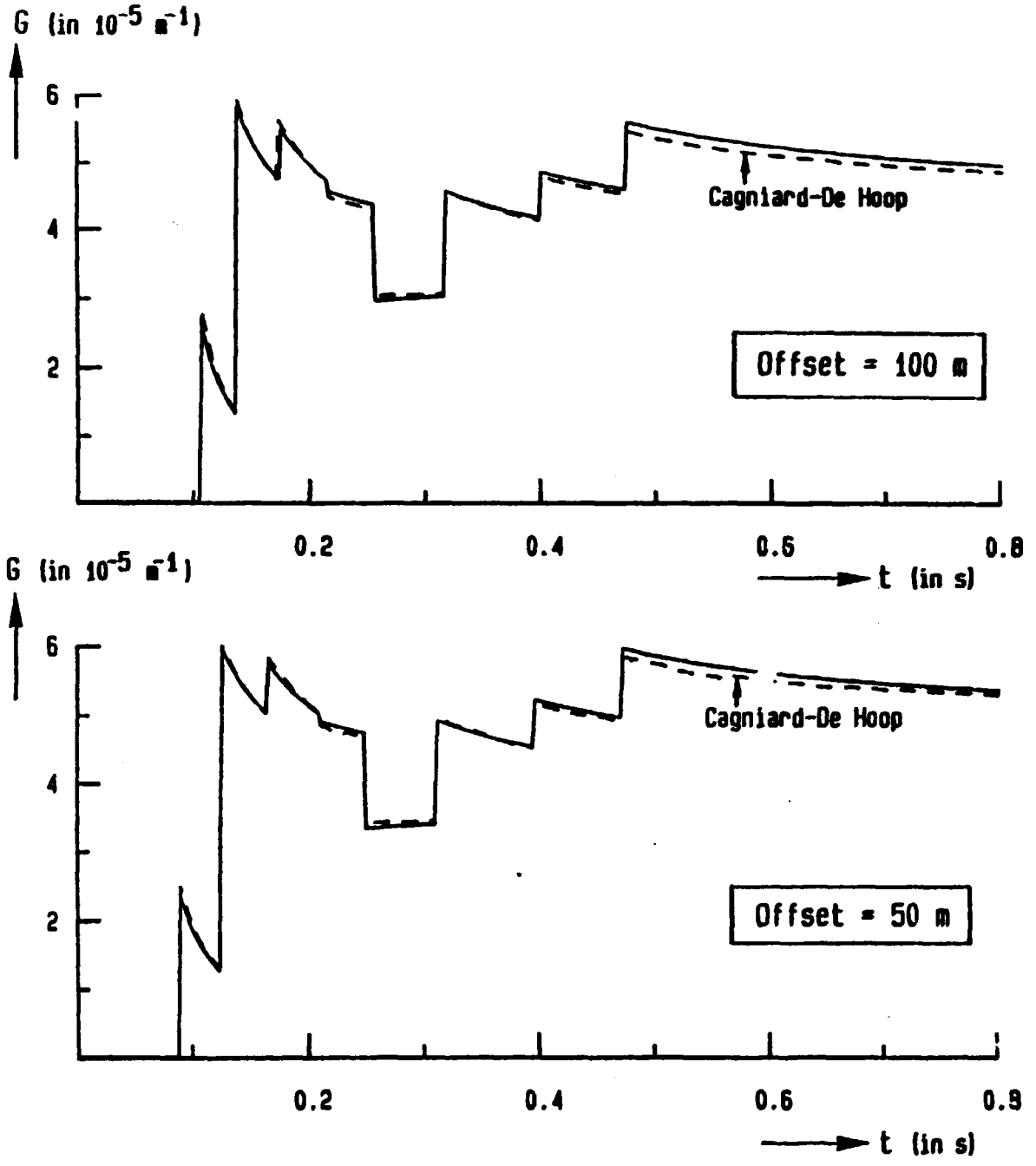

Fig. 3. The RMS Born approximation of the space-time Green's function for the nine-layer configuration of Table 1; $x_3^{(S)} = x_3^{(R)} = 7.5$ m and r = 100 m and r = 50 m, respectively.

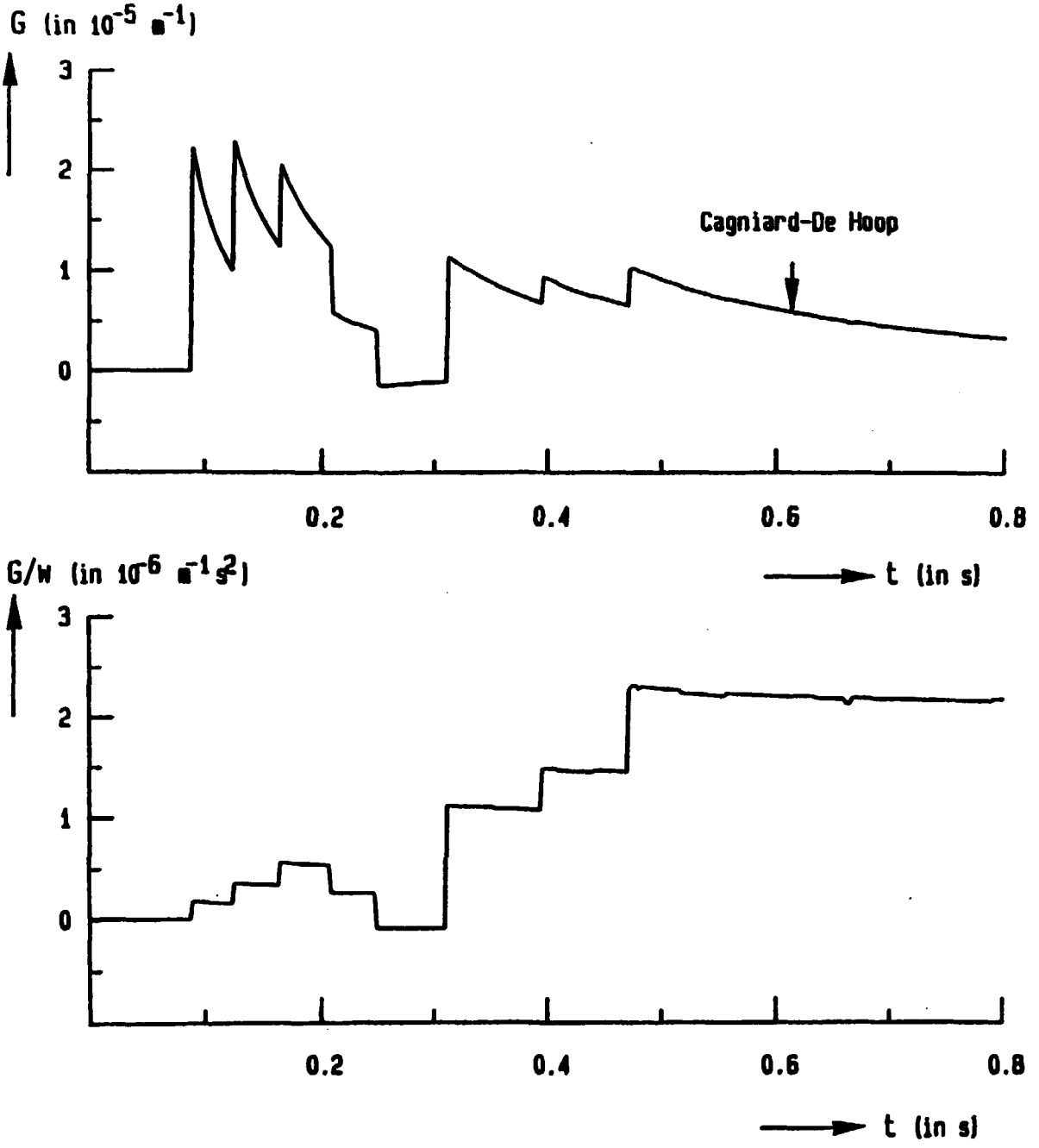

Fig. 4. The results of the space-time Green's function G and G/w for the nine-layer configuration of Table 1, provided $\rho_n = \rho_0$, all n, while $x_3^{(S)} = x_3^{(R)} = 7.5$ m and $r = 50$ m.

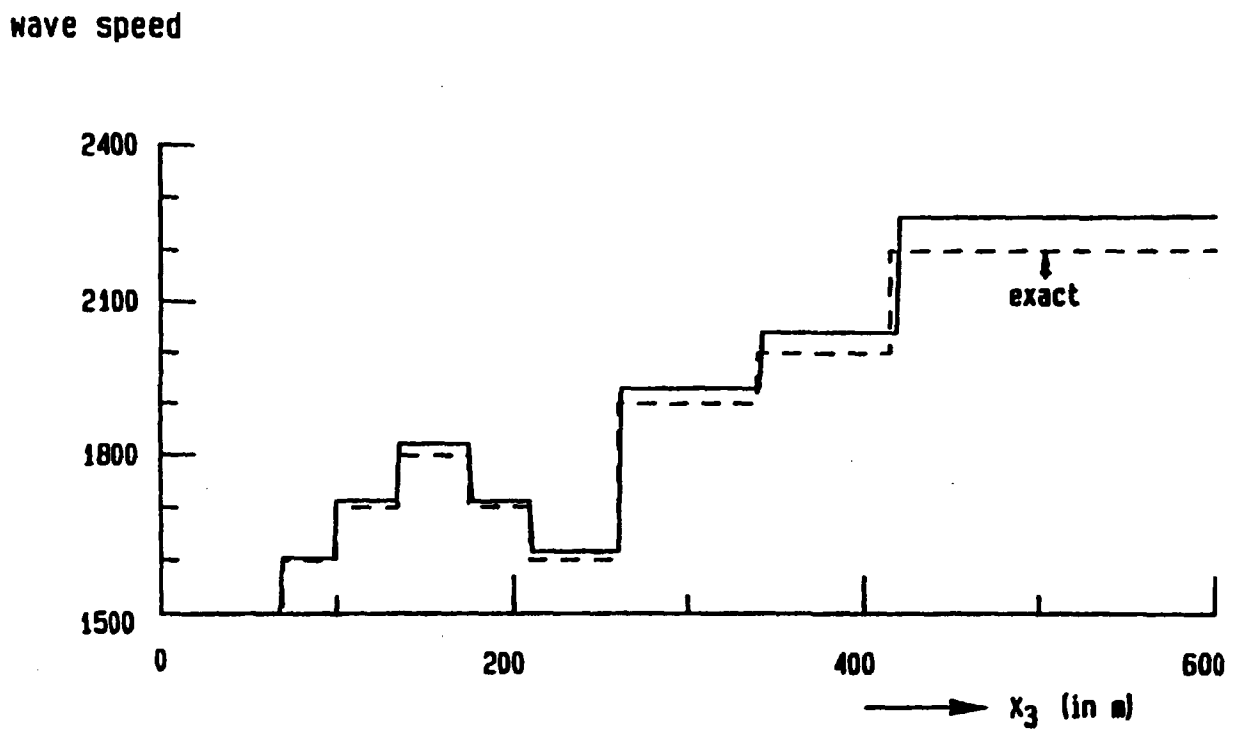

Fig. 5. Reconstructed wave speed c_n from the data of Fig. 4.

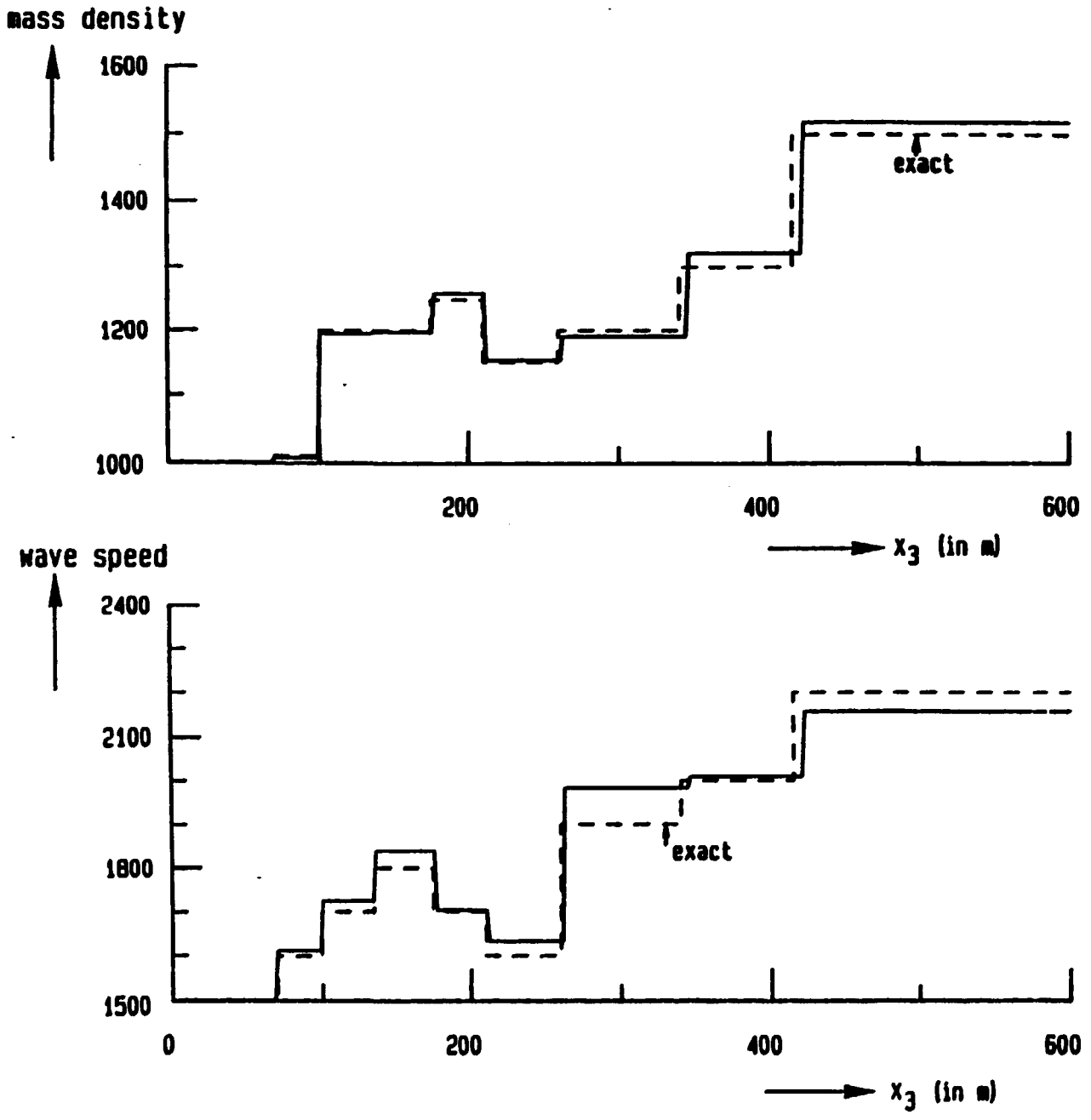

Fig. 6. Reconstructed mass density ρ_n and wave speed c_n from the data of Fig. 3, when $r = 50$ m.

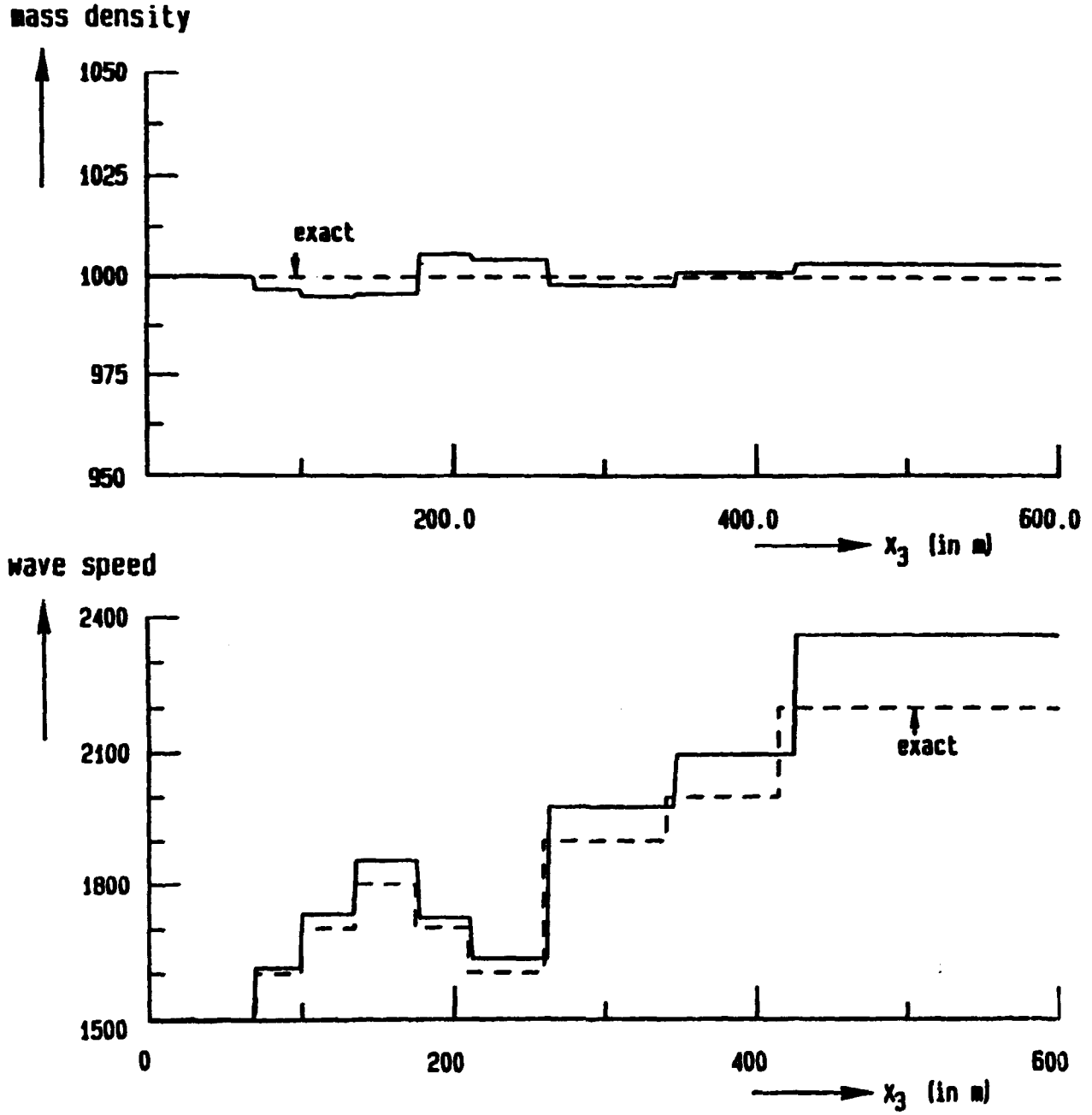

Fig. 7. Reconstructed mass density ρ_n and wave speed c_n from the data of Fig. 4.